NANO LETTERS

xxxx
Vol. 0, No. 0
A−G

Reducing Facet Nucleation during Algorithmic Self-Assembly

Ho-Lin Chen,[†,‡] Rebecca Schulman,[†,§] Ashish Goel,[‡,||] and Erik Winfree*[,§,⊥]

Departments of Computer Science and Computation and Neural Systems, California Institute of Technology, Pasadena, California 91125, and Departments of Computer Science and Management Science and Engineering, Stanford University, Stanford, California 94305

Received April 4, 2007; Revised Manuscript Received July 3, 2007

ABSTRACT

Algorithmic self-assembly, a generalization of crystal growth, has been proposed as a mechanism for bottom-up fabrication of complex nanostructures and autonomous DNA computation. In principle, growth can be programmed by designing a set of molecular tiles with binding interactions that enforce assembly rules. In practice, however, errors during assembly cause undesired products, drastically reducing yields. Here we provide experimental evidence that assembly can be made more robust to errors by adding redundant tiles that "proofread" assembly. We construct DNA tile sets for two methods, uniform and snaked proofreading. While both tile sets are predicted to reduce errors during growth, the snaked proofreading tile set is also designed to reduce nucleation errors on crystal facets. Using atomic force microscopy to image growth of proofreading tiles on ribbon-like crystals presenting long facets, we show that under the physical conditions we studied the rate of facet nucleation is 4-fold smaller for snaked proofreading tile sets than for uniform proofreading tile sets.

Molecular self-assembly is an emerging technology that will ultimately enable the fabrication of great quantities of complex nanoscale objects such as computer circuits at very low cost. The difficulty of self-assembling complex objects lies in the fact that precise direction of assembly in the form of a set of instructions (an algorithm) must be encoded in the molecules themselves. Nucleic acids allow the construction of programmable units for self-assembly,[1] here called "tiles", that have been used to create periodic lattices[2−4] and small finite assemblies.[5−7] Algorithmic self-assembly, a generalized form of crystal growth,[8] has been proposed as a general method for directing the growth of complex finite and infinite objects.[9] In principle, arbitrarily complex objects can be constructed using algorithmic self-assembly,[10] and objects including large finite-sized shapes and some circuit diagrams can be assembled from a small number of components.[11−14] Aperiodic one-[15,16] and two-dimensional[17,18] structures have been algorithmically self-assembled from programmable crystal monomers constructed from DNA tiles.

In algorithmic self-assembly, crystal growth is programmed by designing a set of tiles with binding interactions that enforce specific local assembly rules. Growth begins from a nucleating structure and consists of a series of attachments of single tiles. Under slightly supersaturated conditions, the attachment of a tile to a growing crystal is energetically favorable only if it attaches to a growing crystal by at least two binding sites. The tiles are designed so that during correct assembly, at every step a tile in the pattern attaches by a particular set of two or more binding sites. These binding sites are the tile's *inputs* (Figure 1a): the identities of the binding sites together determine which tile can attach at a given site. In theory, this simple mechanism is sufficient to produce arbitrarily complex shapes and patterns.[9−12] In practice, however, self-assembly is stochastic, and unfavorable attachments of tiles with one or more incorrect or absent inputs also occur.[9,19] While tiles that attach unfavorably usually fall off quickly, occasionally such a tile is locked in by the subsequent favorable attachment of an adjacent tile, an event we will call an *insufficient attachment*. Because a tile that attaches unfavorably may not match some of its input binding sites, it may not be the correct tile in the desired pattern: an error has occurred. Subsequent algorithmic pattern formation can be severely disrupted, resulting in a grossly malformed product.

Figure 1a illustrates correct and erroneous assembly steps. Insufficient attachments at sites where a correct tile could have attached are called *growth errors*; they involve both a correctly matching binding site and a mismatch. Insufficient attachments on facets involve no mismatches; nonetheless,

* Corresponding author. E-mail: winfree@caltech.edu.
† These authors contributed equally to this work.
‡ Department of Computer Science, Stanford University.
§ Department of Computation and Neural Systems, California Institute of Technology.
|| Department of Management Science and Engineering, Stanford University.
⊥ Department of Computer Science, California Institute of Technology.

10.1021/nl070793o CCC: $37.00
Published on Web 08/24/2007

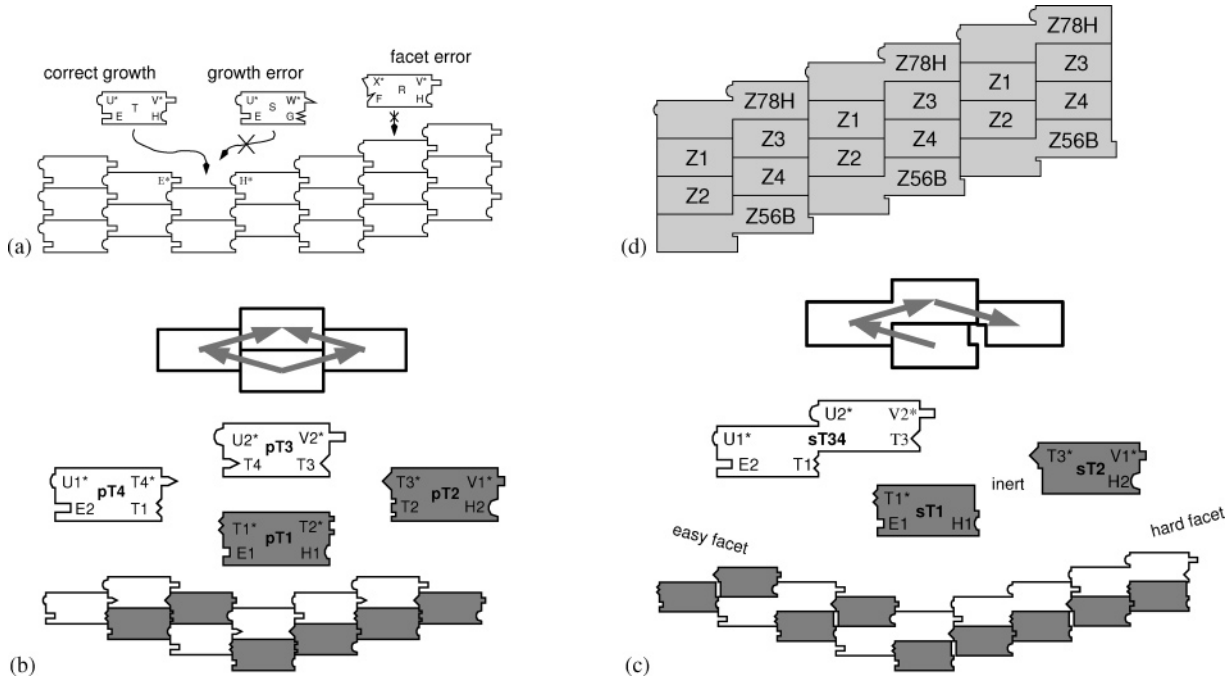

Figure 1. Algorithmic self-assembly and proofreading blocks. (a) During algorithmic self-assembly, a tile attaches to a growing crystal by binding domains on its edges. Here, the four labels on a tile's corners indicate specific binding domains; asterisk indicates complementary domains (X binds to X*). The attachment of a tile where both its input (bottom) edges match the available edges on the crystal is preferred over the attachment of a tile where a single (or no) match occurs. Growth errors occur when a tile attaches by one matching bond and one nonmatching bond. Facet errors occur when a tile attaches by only one matching bond. In both cases, for an error to occur, the incorrect tile must be "locked in" by a second tile before it detaches. (b) The logical structure of a 2×2 uniform proofreading block. Each tile in the original tile set is converted into four tiles that, as a logical block, redundantly encode the same input and output information on the perimeter of the block, while binding domains on the interior of the block encode the identity of the original tile. Correct assembly at a growth site proceeds one tile at a time, either in the order pT1−pT2−pT4−pT3 or in the order pT1−pT4−pT2−pT3. The unique labels inside a proofreading block reduce the rate of growth errors because for a block to be completed, one of the tiles that attaches on top of an incorrect tile must also be incorrect—it cannot match both the label inside the block and the label presented by the crystal. (c) The structure of a 2×2 snaked proofreading block. Binding labels on the perimeter of the block are the same as in a uniform proofreading block, but the interior has two modifications: there is an inert interaction between sT1 and sT2, and the other two tiles are fused to create the "double tile" sT34. This forces correct assembly to proceed in the order sT1−sT34−sT2. Snaked proofreading tile sets, like uniform proofreading tile sets, force a subsequent tile that attaches after an incorrect attachment to be incorrect also. (d) Zigzag ribbons. While only three repeat units are shown, ribbons can be arbitrarily long. The 6 tiles interact through 12 distinct pairwise binding domains, all shown as flat sides, as their logic is not essential here. In addition to the double tiles shown, we use variants of the double tiles that present binding domains to create a desired facet (e.g., Z78H presents H1* and H2* for the hard facet) or present inert "blunt ends" (e.g., Z56B) to which nothing may bind.

the added tiles may be incorrect for the pattern. Therefore, they are called *facet errors*. Unlike standard crystal growth, where nucleation on facets is part of the desired growth process, in a proper algorithmic self-assembly every tile attaches by two or more binding sites. Facet errors were identified as a major source of algorithmic self-assembly errors both in experimental[17] and in theoretical[20,21] studies. The overall rate of errors during assembly is the sum of the growth errors and the facet errors.

The choice of tiles for an algorithmic self-assembly process not only determines the pattern that is formed when all attachments are favorable but also determines the growth path and can influence the rate at which errors occur during growth. In theory, it is possible to transform a less robust tile set into a more robust tile set that can assemble the desired object with fewer errors.[20−23] In such transformed tile sets, a block of tiles plays the same logical role as a single tile in the less robust tile set (Figure 1b). The goal is for such blocks to exploit a form of "proofreading": when an incorrect tile attaches, further unfavorable assembly steps must occur within the block in order for the incorrect tile to become locked in place. Because such steps are rare, assembly stalls, allowing more time for the incorrect tile to fall off, so that correct assembly can proceed.

Simulations of the first proofreading tile sets[20] (Figure 1b), here called *uniform proofreading tile sets*, show a substantial reduction in the rate of *growth errors*. However, uniform proofreading tile sets do not reduce the rate of facet errors; just one insufficient attachment can nucleate the growth of a layer of uniform proofreading tiles along an entire facet (Figure 2a). *Snaked proofreading tile sets*[21] (Figure 1c) improve on uniform proofreading tile sets. They reduce the rate of growth errors in the same way as uniform proofreading tile sets and additionally reduce the rate of facet errors; multiple adjacent insufficient attachments must occur before favorable growth can continue along a facet (Figure 2b). The 2×2 snaked proofreading tile set shown in Figure 1c only protects against facet errors on the facet parallel to the sT1 and sT2 tiles; we call this the "hard facet". The other, "easy", facet theoretically permits facet errors at approximately

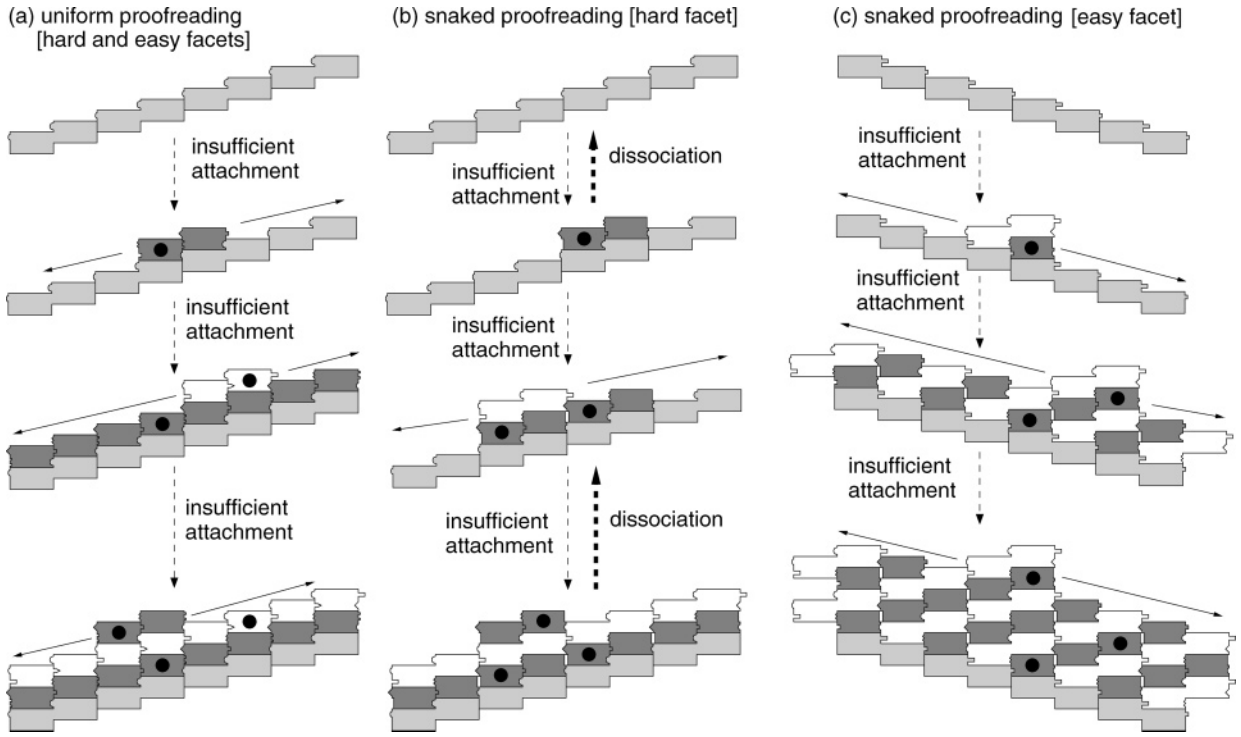

Figure 2. Facet nucleation and growth. (a) Facet nucleation of uniform proofreading blocks. Following a single insufficient attachment (tiles with dots indicate the unfavorable attachments that were locked in), subsequent growth by favorable attachments can grow an entire layer of tiles. Subsequent rows are each nucleated by a single insufficient attachment event. (b) Facet nucleation for snaked proofreading blocks along the hard facet. Here, a single insufficient attachment results in a pair of tiles on the facet, but further favorable growth steps are impossible because of the inert bonds interior to the snaked blocks. Two adjacent insufficient attachments are necessary to nucleate two layers of facet growth. Each additional two layers of growth requires another two adjacent insufficient attachments. (c) Facet nucleation for snaked proofreading blocks along the easy facet. Here, an insufficient attachment consists of a single tile and an adjacent double tile. Thus, two layers of snaked proofreading tiles can be nucleated by just one insufficient attachment.

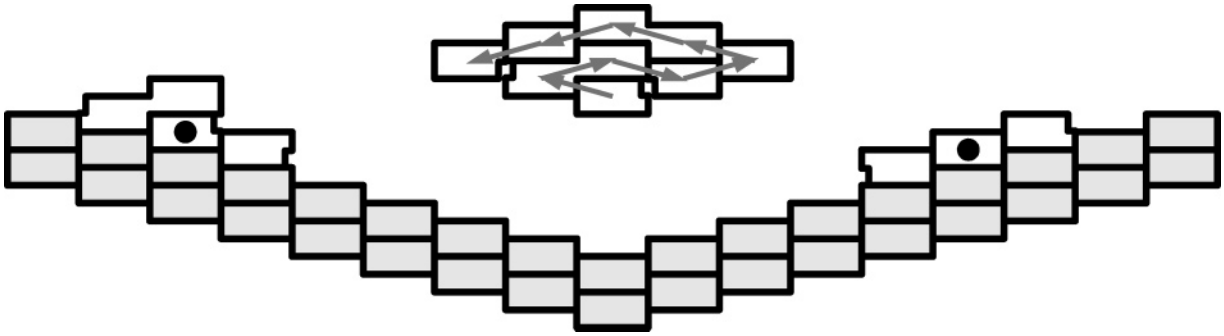

Figure 3. 3 × 3 snaked blocks reduce facet growth on both facet types. On either facet, an isolated insufficient attachment (initiated by the tiles marked with dots) can grow by favorable attachment to a maximal size of three tiles, at which point it is no longer possible to attach a tile by two binding sites. However, at a proper growth site, the series of exclusively favorable assembly steps following the snaked path shown can complete the block quickly.

the same rate as for the uniform proofreading tile set (Figure 2c).

The larger 3 × 3 snaked proofreading block (Figure 3) can protect against facet errors on both facet orientations, as is necessary for the full range of algorithmic growth. Simulation and theory predict that these and larger $k \times k$ blocks further reduce both growth errors and facet errors.[21] The larger blocks use the basic mechanism of the 2 × 2 block multiple times to reduce the rate of facet errors; for example, the 3 × 3 block uses the 2 × 2 snaked motif once for each facet orientation. Thus, experimental investigation of the 2 × 2 system assesses the essential principle used by the larger systems.

In this paper, we investigate experimentally whether 2 × 2 snaked proofreading tiles have a lower rate of facet nucleation than 2 × 2 uniform proofreading tiles. We use DNA tiles (Figure 4) to implement both uniform and snaked proofreading blocks and study their growth on long facets created using zigzag ribbons[24] (Figure 1d). See Supplementary Figures S1−S11 for sequences and diagrams of all molecules used in this work. We show that with snaked proofreading blocks, facet nucleation errors are reduced

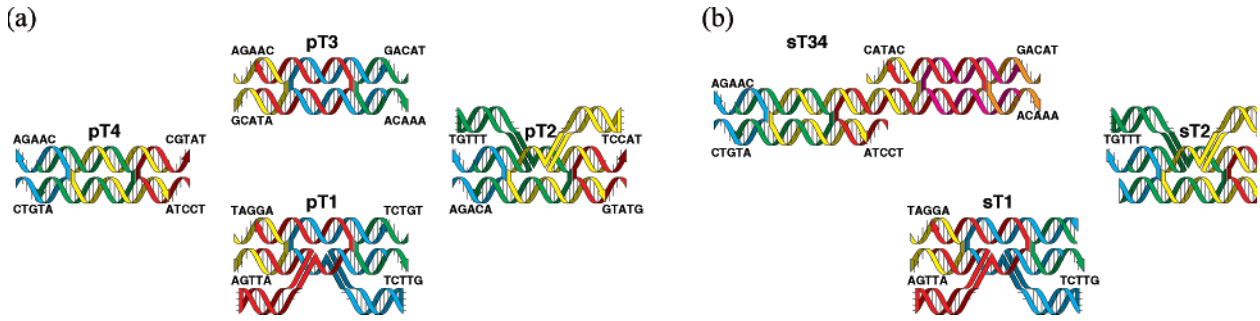

Figure 4. DNA implementation of uniform and snaked proofreading blocks. (a) DNA tiles for a uniform proofreading block. Each tile shown is a double-crossover molecule known as the DAO-E molecule.[25] A DAO-E molecule is composed of four strands of DNA. While the "core" of the molecule is double stranded, there are four five-nucleotide single-stranded regions (sticky ends) on each molecule that can bind to complementary sticky ends on other tiles. Two hairpins are present on each of the shaded tiles in Figure 1b to provide AFM contrast. (b) DNA tiles for a 2 × 2 snaked proofreading block, which in the rest of the paper will be referred to simply as a "snaked proofreading block". To make an inert bond between sT1 and sT2, the sticky ends of the tiles are double stranded and truncated by two and three bases, respectively. The double tile sT34 is implemented by a larger molecule which has the structure of two DAO-E tiles fused together. Hairpins are used on tiles shaded in Figure 1c.

significantly on the expected facet. This demonstrates the effectiveness of the basic principle underlying snaked proofreading.

Results. (A) Lattice Structure. We first verified that the DNA structures we designed to implement uniform proofreading, snaked proofreading, and facets formed as expected. We used gel electrophoresis to verify that each of the four tiles in both proofreading tile sets assembled correctly. The component strands for each tile were annealed in a PCR machine (Eppendorf) from 90 to 20 °C at a rate of 0.1 °C every 6 s. Nondenaturing gel electrophoresis of the annealed tiles showed that the strands for each of the tiles in Figure 4 formed a single product with at least 80% yield. To make lattices, we mixed the annealed tiles for each lattice at room temperature to a final concentration of 100 nM per strand. We waited for half an hour and then deposited the samples onto mica and imaged by tapping mode atomic force microscopy (AFM). Both the uniform and proofreading tiles formed lattices (Figure 5a,c). (Compared to simply annealing all strands together in one step, this procedure is known to result in smaller and poorly formed crystals, but it is closer to the conditions used in experiments to measure facet nucleation.) The bright stripes in every other row of tiles confirmed that the tiles in the lattices were arranged correctly.

We determined the annealing and melting temperatures of each lattice using measurements of 260 nm absorbance[26] made by a spectrophotometer with a computer-controlled temperature bath (AVIV Biomedical) during an anneal and subsequent melt. The strands for each lattice (50 nM per strand) were annealed from 90 to 10 °C over 10 h, held at 10 °C for 2 h, and then melted back to 90 °C at the same rate. For both lattices, we observed (Figure 12 in Supporting Information) a reversible transition between 45 and 70 °C, where tile formation has been observed previously,[3,17,24] and a hysteretic transition at lower temperatures, where lattices formed. Formation of both lattices occurred around 16 °C and melted between 25 and 37 °C, indicating a significant kinetic barrier to homogeneous nucleation. As ribbons would lower this kinetic barrier, we expected that in the presence of ribbons at room temperature, lattices would grow on ribbons rather than nucleating spontaneously. At lower temperatures during melting, the uniform proofreading lattice absorbance signal was very noisy (presumably due to light scattering that occurs when the lattices grow larger than the 260 nm wavelength being measured), but it appears that the uniform proofreading lattices melted at a temperature ~3 °C higher than the snaked proofreading lattices.

Having demonstrated that the DNA implementation of both proofreading blocks can form crystalline lattices, and are thus structurally sound for investigating their relative effectiveness for reducing assembly errors, we proceeded to construct four types of zigzag ribbon, each of which presents a different combination of one of three facet types: "easy," where snaked proofreading tiles can nucleate growth with just one insufficient attachment; "hard," where two adjacent insufficient attachments are required for snaked proofreading tiles to nucleate facet growth; or blunt, which contain no binding sites and therefore do not allow growth. The "ZZeasy" ribbon has sticky ends for the easy facet (E1* and E2*) on the Z78 tile and blunt sticky ends on the Z56 tile, while the "ZZhard" ribbon has sticky ends for the hard facet (H1* and H2*) on the Z78 tile and blunt sticky ends on the Z56 tile. To directly compare the rates of facet nucleation on the two facet types within the same experiment, we used ribbons with a distinct facet type on each side of the ribbon so that we could compare the number of layers that grow on each side. The "ZZeasyhard" ribbon presents the easy facet on the Z78 tile and the hard facet on the Z56 tile, while the "ZZhardeasy" ribbon presents the hard facet on the Z78 tile and the easy facet on the Z56 tile.

To assemble each of the four ribbon types used to create the desired facets, we annealed their component tiles as described above and then mixed them together at room temperature to a final concentration of 100 nM of each tile. We annealed this mixture from 60 to 20 °C with the temperature decreasing 0.1 °C per minute. AFM imaging after dilution to 10 nM showed that each ribbon type formed four-tile-wide zigzag ribbons with a typical length of several micrometers (Figure 5b).

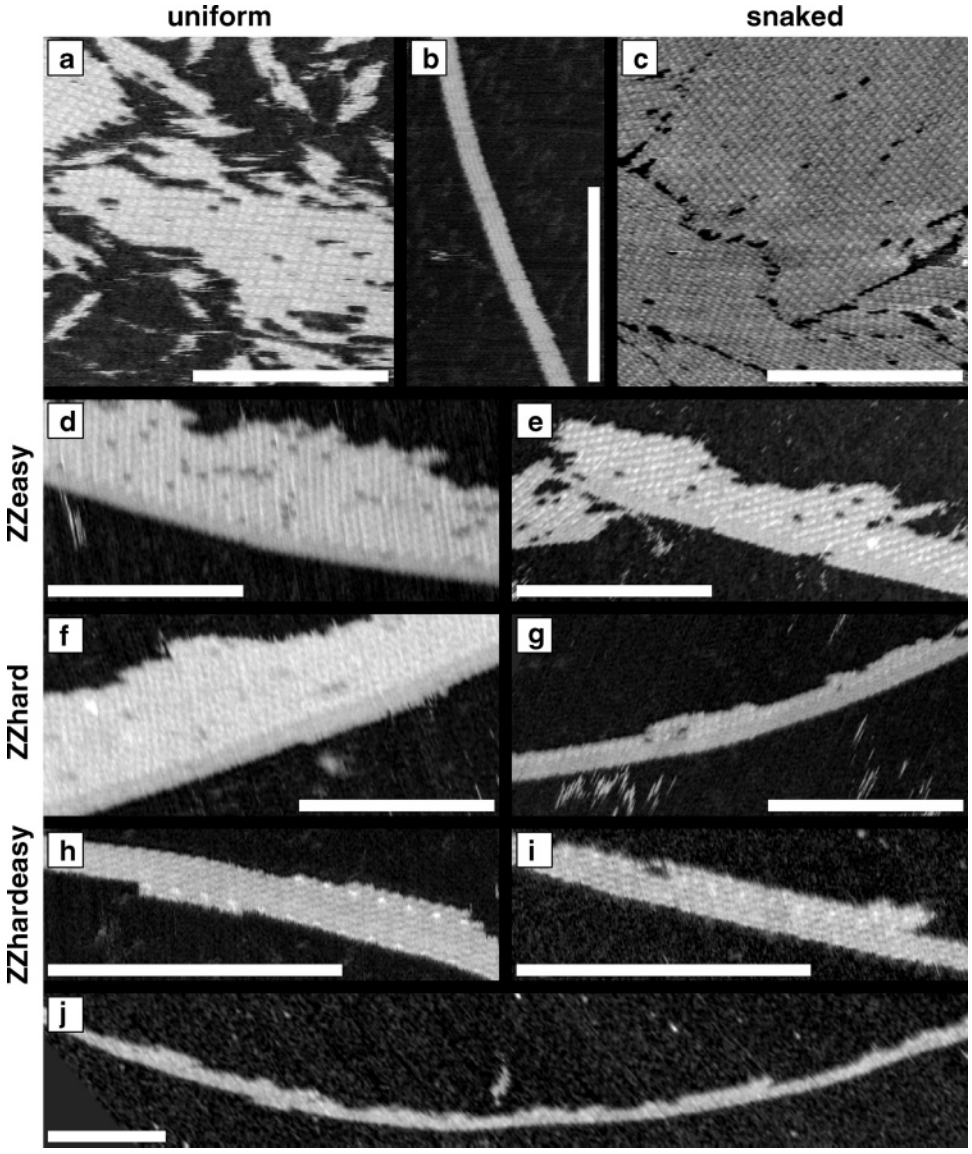

Figure 5. AFM images. Missing tiles are due to damage during AFM scanning. Scale bars are 300 nm. (a) Uniform proofreading lattices (100 nM). (b) Zigzag ribbons, ZZhardeasy (10 nM). (c) Snaked proofreading lattices (100 nM). (d) ZZeasy (10 nM) with uniform proofreading (50 nM). (e) ZZeasy (10 nM) with snaked proofreading (50 nM). (f) ZZhard (10 nM) with uniform proofreading (50 nM). (g) ZZhard (10 nM) with snaked proofreading (50 nM). (h) ZZhardeasy (10 nM) with uniform proofreading (10 nM). (i) ZZhardeasy (10 nM) with snaked proofreading (10 nM). (j) A long ZZhardeasy ribbon with snaked proofreading.

(B) Facet Growth on Single-Sided Ribbons. We used single-sided ribbons to measure the rate at which lattices grow on a facet. Since each row of growth must be nucleated by one or more insufficient attachments (Figure 2), the number of rows that grow on a facet in a fixed period of time increases with increasing nucleation rate. For each kind of proofreading lattice, we assembled ribbons that presented either an easy or hard facet as described above and then diluted them to 10 nM. We immediately added 50 nM of each preformed proofreading tile, waited for 10 min, then deposited the samples onto mica and imaged them using AFM.

Both kinds of proofreading lattices grew on both facets (parts d−g of Figure 5). The uniform proofreading lattices grew more than 10 layers on both facets, as did the snaked proofreading lattice on the easy facet. In contrast, the snaked proofreading lattice grew only two to six rows on the hard facet during the experiment, suggesting that the nucleation rate of the snaked proofreading lattice on the facet is less than that of the other cases. However, because most of the tiles were used up during the experiment (50 nM is enough to grow an average of 10 rows on each ribbon), it was not possible to quantify how much smaller the nucleation rate of snaked proofreading lattices on the hard facet is than the other rates. Reliability was also limited by trial-to-trial variations in experiment timing and in tile stoichiometry for both the lattices and the ribbons and by concerns about the difference in the melting temperatures of the two lattices.

(C) Facet Growth on Double-Sided Ribbons. We therefore devised a second set of experiments to quantitatively compare the relative growth rates of the two kinds of proofreading lattices on both easy and hard facets. In these

Table 1. Ratio of the Number of Tiles (or Number of Groups of Tiles) Attached on the Easy Facet to the Number of Tiles Attached on the Hard Facet, As Measured from the AFM Data[a]

easy/hard ratio	ZZhardeasy	ZZeasyhard
uniform proofreading	tiles: 1.0 ± 0.2	tiles: 1.2 ± 0.2
	groups: 1.1 ± 0.2	groups: 1.5 ± 0.3
snaked proofreading	tiles: 4.8 ± 1.0	tiles: 3.9 ± 0.9
	groups: 4.8 ± 1.0	groups: 4.2 ± 0.9

[a] Error bars indicate 1 standard deviation and are calculated using bootstrapping.

experiments, we measured the growth rate of the lattices on zigzag ribbons that present an easy facet on one side and a hard facet on the other. Because growth on both kinds of facets occurs under exactly the same physical conditions with identical thermodynamics on both sides, the ratio of growth on the two facets accurately measures the preference for growth on one facet over another. Growth on the easy and hard facet can be distinguished under the AFM because the orientation of stripes in the lattice with respect to the ribbon is different on the two sides (parts d−g of Figure 5).

For each lattice type, we performed experiments with double-sided ribbons using the same procedure as for the single-sided zigzag ribbons above. Experiments where we added 50 nM of proofreading tiles to the ZZeasyhard ribbons produced aggregations of ribbons in which lattices growing off each side merged with those of other ribbons, and it was not possible to measure the relative growth rate of tiles on the two facets. Aggregation was not a problem when we used a lower concentration, 10 nM, of proofreading tiles. To ensure that unknown structural differences between the Z78 and Z56 tiles used on either side of the ribbons did not affect the attachment rate, we repeated the competition experiment with both kinds of proofreading tiles at 10 nM with double-sided ribbons where the facet types were placed on opposite sides of the ribbon (ZZhardeasy). For each of the four experiments, we counted the number of tiles and groups that grew on each side of approximately 25 μm of ribbon (parts h−j of Figure 5). (A group is a connected assembly of two rows of tiles that could have grown as a result of a single nucleation event.) The results (Table 1) quantitatively confirm the conclusions of the earlier experiment. Only snaked proofreading tiles prefer to attach to the easy facet. In both experiments with snaked proofreading tiles, there were at least four times more snaked proofreading tiles attached to the easy facet.

(D) Analysis. These experimental results may be compared with a kinetic Monte Carlo model of DNA tile crystal growth, the kinetic Tile Assembly Model (kTAM).[9] In this model, a tile bound by a single sticky end will dissociate with rate $r_1 = k_f\, e^{\Delta G^\circ_1/RT}$, a tile bound by two sticky ends will dissociate with rate $r_2 = k_f\, e^{\Delta G^\circ_2/RT}$, while tiles arrive at a given site at rate $f = k_f\, C$, where C is the concentrations of free monomer tiles in solution. For the tiles used here, k_f, ΔG°_1, and ΔG°_2 are not known but can be estimated based on the sticky end sequences, a nearest neighbor model of DNA thermodynamics,[27] and the kinetics of oligonucleotide hybridization.[28] We ran kTAM simulations of snaked tile growth on easy and hard facets during 10 min with $C = 10$ nM, $\Delta G^\circ_1 = \Delta G^\circ_{se} + \Delta G^\circ_{init}$ and $\Delta G^\circ_2 = 2\Delta G^\circ_{se} + \Delta G^\circ_{init}$ with $\Delta G^\circ_{se} = -10.3$ kcal/mol and an entropic $\Delta G^\circ_{init} = 1.8$ kcal/mol at 25 °C, and $k_f = 17 \times 10^6$/M/s (chosen to obtain a comparable total extent of growth within 10 min). The simulated easy/hard ratio was 5.7 ± 0.6. While this is remarkable agreement with our data, the simulation results are quite sensitive to ΔG°_{se} and ΔG°_{init}, which we do not know with confidence. (The nucleation rate ratio is relatively unaffected by k_f.)

The simulations suggest that much better ratios could be achieved at higher temperatures, closer to T_m for the lattice, as can be understood using a simplified analytic model. The rate of an insufficient attachment, which is sufficient for nucleation with uniform proofreading and on the easy facet with snaked proofreading, is approximated as a two-step process[21]

$$\mathrm{E} \underset{r_1}{\overset{f}{\rightleftharpoons}} \mathrm{S} \xrightarrow{f} \mathrm{IA}$$

where E is an empty site on a facet, S indicates attachment of a single isolated tile, and IA indicates an insufficient attachment has occurred. Thus,

$$k_{IA} \approx \frac{f(f+r_1)}{(f+(f+r_1))}\frac{f}{(f+r_1)}$$

where the first term is the overall rate for the two steps E → S followed by S → IA or S → E, and the second term is the probability that IA was reached in that cycle. Similarly, on the hard facet with snaked proofreading, nucleation takes place when two insufficient attachments occur next to each other:

$$\mathrm{E} \underset{r_2}{\overset{k_{IA}}{\rightleftharpoons}} \mathrm{IA} \xrightarrow{k_{IA}} \mathrm{NUC}$$

yielding

$$k_{NUC} \approx \frac{k_{IA}(k_{IA}+r_2)}{k_{IA}+(k_{IA}+r_2)}\frac{k_{IA}}{(k_{IA}+r_2)}$$

Near T_m, where $f \approx r_2$, we have $r_1 \gg f$ and $k_{IA} \approx f(f/r_1) \approx f e^{(\Delta G^\circ_2 - \Delta G^\circ_1)/RT} = f e^{\Delta G^\circ_{se}/RT}$. Thus, $r_2 \gg k_{IA}$ so $k_{NUC} \approx k_{IA}(k_{IA}/r_2)$. Consequently, the ratio of nucleation rates on the easy and hard facets is approximately $k_{IA}/k_{NUC} \approx r_2/k_{IA} \approx e^{-\Delta G^\circ_{se}/RT}$. For a concentration $C = 10$ nM, at T_m we have $\Delta G^\circ_{se} \approx -6.4$ kcal/mol (as calculated based on $f \approx r_2$ and hence $\Delta G^\circ_2 = RT \ln C$; the sticky end bonds will be weaker than those at 25 °C), but this still provides a remarkably favorable ratio of nucleation rates. By contrast, without the simplifications that apply near T_m, these formulas predict that the ratio decreases quickly as sticky end bonds become stronger, dropping to moderate values as the experimental conditions are approached. (This simplified theory predicts lower nucleation rates than those obtained in the simulations, however.)

For a tile set to be effective at reducing error rates in algorithmic self-assembly, not only must it reduce facet nucleation errors and growth errors, but proper growth must proceed unhindered. In kTAM simulations, both proofreading tile sets grow at roughly the same rate at growth sites, since there is always a location where a tile can attach by two binding sites. According to the simplified theory, growth at proper attachment sites, $k_{GROW} = f - r_2$, also decreases as T_m is approached, but k_{IA} and k_{NUC} decrease much more quickly, so that near T_m gives the most favorable ratio of growth to facet nucleation.

The use of these models for quantitative predictions is limited by our lack of accurate parameters for the full kTAM and by the nature of approximations used in the simplified analytic model. For example, ΔG_1° could be different for each sticky end sequence and ΔG_2° might not be a simple sum if steric effects come into play. Furthermore, it is possible that the favorable energy of blunt end stacking[29] between sT1 and sT2 needs to be taken into account; our model neglects it. There may also be small but nonzero energies between nonmatching sticky ends as well as stoichiometry imbalance among the tile types. Errors in the simplified analytic model, relative to the kTAM, arise due to the complexities of the crystal growth process, such as the combinatorial multiplicity of growth pathways, that are difficult to incorporate in a simple theory. Despite these caveats, we believe that the simulation and model provide valuable insights that can explain and guide experimental studies, for example, by suggesting how to change experimental conditions to obtain better performance.

Conclusions. We have shown here that snaked proofreading tiles reduce the rate of tile growth on long facets by at least a factor of 4 at 25 °C. Thus, we conclude that the snaked proofreading blocks reduce facet nucleation as designed, confirming the soundness of the basic principle of snaked proofreading. Presuming that growth at proper growth sites proceeds at comparable rates for both tile sets, which is not inconsistent with the extent of growth observed on ribbons, this suggests that in algorithmic growth the rate of errors per tile should be reduced. An important future experiment would be to verify this prediction. Another important direction is to determine how much error rates improve at optimal algorithmic assembly conditions, close to the melting temperature of the lattices. More generally, however, these results suggest that logical redesign of a set of tiles can reduce errors and that control over the growth path for self-assembly can be used to selectively inhibit undesired assembly processes. The general concept of robust proofreading tile sets is therefore worthy of further experimental and theoretical study.

Acknowledgment. We thank Paul Rothemund and an anonymous referee for useful comments and discussions. E.W. acknowledges National Science Foundation (NSF) awards 0093486 and 0432193. E.W. and A.G. acknowledge NSF award 0523761. A.G. acknowledges NSF awards 0339262 and 0323766.

Supporting Information Available: Description of experimental methods, diagrams for the DX molecules used, sequences for all DNA strands, and UV melting data. This material is available free of charge via the Internet at http://pubs.acs.org.

References

(1) Seeman, N. C. *J. Theor. Biol.* **1982**, *99*, 237−247.
(2) Winfree, E.; Liu, F.; Wenzler, L. A.; Seeman, N. C. *Nature* **1998**, *394*, 539−544.
(3) LaBean, T. H.; Yan, H.; Kopatsch, J.; Liu, F.; Winfree, E.; Reif, J. H.; Seeman, N. C. *J. Am. Chem. Soc.* **2000**, *122*, 1848−1860.
(4) He, Y.; Chen, Y.; Liu, H.; Ribbe, A. E.; Mao, C. *J. Am. Chem. Soc.* **2005**, *127*, 12202−12203.
(5) Chworos, A.; Severcan, I.; Koyfman, A. Y.; Weinkam, P.; Oroudjev, E.; Hansma, H. G.; Jaeger, L. *Science* **2004**, *306*, 2068−2072.
(6) Lund, K.; Liu, Y.; Lindsay, S.; Yan, H. *J. Am. Chem. Soc.* **2005**, *127*, 17606−17607.
(7) Liu, Y.; Ke, Y.; Yan, H. *J. Am. Chem. Soc.* **2005**, *127*, 17140−17141.
(8) Davey, R.; Garside, J. *From Molecules to Crystallizers*; Oxford University Press: Oxford, U.K., 2000.
(9) Winfree, E. *Simulations of Computing by Self-Assembly*; Technical Report CS-TR:1998.22; Caltech: Pasadena, CA, 1998.
(10) Soloveichik, D.; Winfree, E. *SIAM J. Comput.* **2007**, *36*, 1544−1569. Extended abstract in LNCS 3384: 344−354 (2004); preprint is cs.CC/0412096 on arXiv.org.
(11) Rothemund, P. W. K.; Winfree, E. The program-size complexity of self-assembled squares. In *Symposium on Theory of Computing* (*STOC*); ACM Press: Portland, OR, 2000.
(12) Adleman, L. M.; Cheng, Q.; Goel, A.; Huang, M.-D. *Symposium on the Theory of Computing* (*STOC*); ACM Press: Portland, OR, 2001.
(13) Cook, M.; Rothemund, P. W. K.; Winfree, E. Self-Assembled Circuit Patterns. In *DNA Computing 9*, Vol. LNCS 2943; Chen, J.; Reif, J., Eds.; Springer-Verlag: Berlin and Heidelberg, 2004.
(14) Aggarwal, G.; Cheng, Q.; Goldwasser, M. H.; Kao, M.-Y.; de Espanes, P. M.; Schweller, R. T. *SIAM J. Comput.* **2005**, *34*, 1493−1515. An extended abstract of this work appeared in the *Proceedings of the ACM/SIAM Symposium on Discrete Algorithms* (*SODA*), 2004, pp 880−889.
(15) Adleman, L. M. *Science* **1994**, *266*, 1021−1024.
(16) Mao, C.; LaBean, T. H.; Reif, J. H.; Seeman, N. C. *Nature* **2000**, *407*, 493−496.
(17) Rothemund, P. W. K.; Papadakis, N.; Winfree, E. *PLoS Biol.* **2004**, *2*, 424−436.
(18) Barish, R. D.; Rothemund, P. W. K.; Winfree, E. *Nano Lett.* **2005**, *5*, 2586−2592.
(19) Baryshnikov, Y. M.; Coffman, E. G.; Seeman, N. C.; Yimwadsana, T. Self-correcting Self-assembly: Growth Models and the Hammersley Process. In *DNA Computing 11*, Vol. LNCS 3892; Carbone, A., Pierce, N. A., Eds.; Springer-Verlag: Berlin and Heidelberg, 2006.
(20) Winfree, E.; Bekbolatov, R. Proofreading Tile Sets: Error-Correction for Algorithmic Self-Assembly. In *DNA Computing 9*, Vol. LNCS 2943; Chen, J., Reif, J., Eds.; Springer-Verlag: Berlin and Heidelberg, 2004.
(21) Chen, H.-L.; Goel, A. Error Free Self-Assembly using Error Prone Tiles. In *DNA Computing 10*, Vol. LNCS 3384; Ferretti, C., Mauri, G., Zandron, C., Eds.; Springer-Verlag: Berlin and Heidelberg, 2005.
(22) Fujibayashi, K.; Murata, S. A method of error suppression for self-assembling DNA tiles. In *DNA Computing 10*, Vol. LNCS 3384; Ferretti, C., Mauri, G., Zandron, C., Eds.; Springer-Verlag: Berlin and Heidelberg, 2005.
(23) Reif, J. H.; Sahu, S.; Yin, P. Compact Error-Resilient Computational DNA Tiling Assemblies. In *DNA Computing 10*, Vol. LNCS 3384; Ferretti, C., Mauri, G., Zandron, C., Eds.; Springer-Verlag: Berlin and Heidelberg, 2005.
(24) Schulman, R.; Winfree, E. Synthesis of crystals with a programmable kinetic barrier to nucleation. *Proc. Natl. Acad. Sci. U.S.A.*, to appear.
(25) Fu, T.-J.; Seeman, N. C. *Biochemistry* **1993**, *32*, 3211−3220.
(26) Bloomfield, V. A.; Crothers, D. M.; Tinoco, I., Jr. *Nucleic Acids: Structures, Properties, and Functions*; University Science Books: Sausalito, CA, 2000.
(27) SantaLucia, J., Jr. *Proc. Natl. Acad. Sci. U.S.A.* **1998**, *95*, 1460−1465.
(28) Morrison, L. E.; Stols, L. M. *Biochemistry* **1993**, *32*, 3095−3104.
(29) Vasiliskov, V. A.; Prokopenko, D. V.; Mirzabekov, A. D. *Nucleic Acids Res.* **2001**, *29*, 2303−2313.

NL070793O